Probing adsorbate dynamics with chirped laser pulses in a single-pulse scheme

F. Steeb,[1] S. Mathias,[1] M. Wiesenmayer,[2] A. Fischer,[1] M. Aeschlimann,[1] M. Bauer,[2,*,†] and J. P. Gauyacq[3,4,*,‡]
[1]*Department of Physics and Research Center OPTIMAS, University of Kaiserslautern, 67663 Kaiserslautern, Germany*
[2]*Institut für Experimentelle und Angewandte Physik, Christian-Albrechts-Universität zu Kiel, 24118 Kiel, Germany*
[3]*CNRS, Institut des Sciences Moléculaires d'Orsay, ISMO, UMR 8214, Bâtiment 351, 91405 Orsay Cedex, France*
[4]*Université Paris-Sud, Institut des Sciences Moléculaires d'Orsay, ISMO, UMR 8214, Bâtiment 351, 91405 Orsay Cedex, France*
(Received 18 June 2010; revised manuscript received 31 August 2010; published 18 October 2010)

Femtosecond dynamics of the model-like adsorption system Cs/Cu(111) is probed by two-photon photoelectron spectroscopy (2PPE) using phase-modulated (chirped) laser pulses. The experimental data are quantitatively modeled within a wavepacket propagation approach under explicit consideration of the adsorbate motion. The results enable us to assign characteristic chirped-pulse 2PPE features to the ultrafast adsorbate dynamics associated with the excited state lifetime and the adsorbate motion, and to improve on the qualitative interpretation of experimental data as published in Petek *et al.* [J. Phys. Chem. A **104**, 10234 (2000)]. Our results show that nonlinear photoemission with a chirped pulse in a single-pulse scheme can complement real-time studies based on pump-probe schemes to gain quantitative insights into the femtosecond dynamics of ultrafast surface processes.

DOI: 10.1103/PhysRevB.82.165430 PACS number(s): 78.47.J−, 79.60.−i, 82.53.St

I. INTRODUCTION

The ultrafast dynamics of surface localized electronic excitations has been studied intensively in the past particularly due to its relevance for the understanding of fundamental aspects regarding surface chemical processes.[1] Within numerous two-photon photoemission (2PPE) studies and time-resolved 2PPE (TR-2PPE) studies, dephasing, and population decay of such excitations have been addressed with a temporal resolution in the femtosecond range (for an overview see, for instance, Refs. 2–6). Image-potential states supported by localized band gaps of metallic surfaces yield a model system very attractive in this context as they can be studied in the frequency domain as well as in the time domain. Well prepared surfaces support such image-potential states, which are barely distorted by inhomogeneous broadening effects, so that a linewidth analysis can provide valuable information about the total dephasing time of these excitations.[7–9] The relatively long lifetime of image potential states makes also real-time measurements highly attractive, which enable one to discriminate between pure dephasing processes and the inelastic decay of the excitation.[10–12] Adsorbate excitations, in contrast, often exhibit a considerable inhomogeneous contribution to the line profile so that lifetime measurements in the frequency domain are very restricted. Furthermore, under chemisorption conditions, the strong coupling of adsorbate excitations to the substrate lowers the typical lifetime into the low femtosecond to attosecond regime. This time regime is, yet, challenging for real-time measurements based on conventional optical pump-probe schemes.

In a recent study of the model adsorption system Cs/Cu(111) Petek *et al.*[13] showed that *phase-modulated* femtosecond laser pulses used in a 2PPE experiment can probe ultrafast processes in the adsorbate-surface interaction in a complementary manner. A characteristic response of the spectral signatures of a Cs^* resonance state to the phase applied to the laser pulse was attributed to the effect of the cesium adsorbate motion taking place on a femtosecond time scale. Even more, the authors interpreted their data in terms of a quantum control of the adsorbate wavepacket by the phase modulation of the excitation pulse.

In the present study, we report on a joint theoretical-experimental study of 2PPE from Cs/Cu(111) with phase modulated femtosecond laser pulses. The theoretical model is based on a wave-packet propagation model that has been successfully applied in several works to the description of ultrafast processes of alkali adsorption systems in the past. Our calculations are complemented by 2PPE experiments, which were performed over an extended phase modulation regime in comparison to Ref. 13. In addition to group-velocity-dispersion (GVD) effects, we considered third-order-dispersion (TOD) effects, following an earlier 2PPE study of the Shockley Surface state of Cu(111) using chirped laser pulses where the importance of TOD has been evidenced.[14] The experimentally observed changes in the peak energy of the Cs^* resonance state as function of the applied phase modulation are quantitatively described by theory in a highly satisfactory manner. We find that the 2PPE signal contains substantial information on the femtosecond dynamics associated both with the decay of the Cs^* resonance state and with the Cs nucleus motion induced by the excitation. 2PPE experiments (in a single-pulse scheme) with phase-modulated laser pulses obviously provide an additional means to study ultrafast surface processes complementary to two-pulse correlation experiments. Furthermore, the high sensitivity of the present approach for the short resonance lifetimes that we observe in the calculated 2PPE spectra indicates that this technique can provide a temporal resolution in the low femtosecond regime.

II. EXPERIMENTAL

A. Experimental setup

Details of the two-photon photoemission experiment using phase-modulated (chirped)[15] laser pulses (hereafter re-

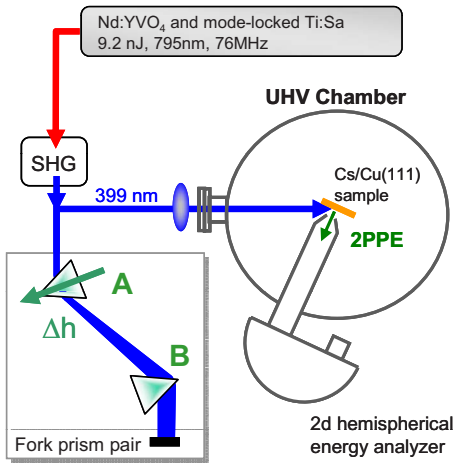

FIG. 1. (Color online) Experimental setup used for the CP-2PPE measurements. GVD and TOD of the SHG laser pulses are adjusted by the translation Δh of the first prism (prism A) of a fork prism pair. The chirped pulses are focused onto the Cs/Cu(111) sample in an UHV chamber. The photoemitted electrons are detected with a 2D hemispherical electron energy analyzer.

ferred to as "chirped-pulse 2PPE" or CP-2PPE) as well as a complete determination of the laser pulse characteristics are described in Ref. 14. Figure 1 shows the scheme of the used experimental setup. A mode-locked Ti:Sapphire laser delivers linearly polarized, transform-limited pulses [center wavelength: 795 nm, spectral width: 46 nm full width at half maximum (FWHM)], which are frequency doubled in a beta barium borate crystal (200 μm thickness) to 399 nm ($h\nu$ =3.11 eV). The bandwidth of the frequency doubled [second-harmonic generation (SHG)] light is 8.7 nm FWHM, supporting a transform-limited pulse duration of $\tau_{TL} \approx 27$ fs.

The spectral phase modulation of the SHG pulses is achieved by the use of a Fork prism pair setup.[16,17] This scheme can be considered as a single-parameter phase modulator that allows a defined control of the second-order spectral phase GVD accompanied by a simultaneous change in the TOD (Ref. 18) of the pulses by a translation Δh of prism A with respect to the laser beam as indicated by the arrow in Fig. 1. In the experiment, fused silica prisms are used with an apex angle of 68.7°. A separation of the two prisms of 51 cm guarantees a zero net GVD of the pulses at the sample position in the ultrahigh vacuum chamber when the beam passes the center of the adjustable prism A. In the following this prism position is referred to as the *zero position* [i.e., GVD(Δh=0 mm)=0 fs^2]. A translation of prism A by $\Delta h = \pm 1$ mm results in a net GVD of ± 368 fs^2,[19–22] where positive values for Δh correspond to an increase of glass in the beam and positive net GVD. Overall, a total GVD range of ± 1500 fs^2 can be spanned with the Fork prism pair configuration. The third-order dispersion of the pulses at the sample position has been determined following a fitting procedure described in an earlier publication.[14] At the zero position of the fork prism pair, the pulses exhibit a TOD =-8000 fs^3 (in the following this value is referred to as TOD$_0$). A translation of prism A by $\Delta h = \pm 1$ mm results in a change in the TOD contribution by ± 114 fs^3. Overall, the spectral GVD and TOD phase modulation $\psi(\omega, \Delta h)$ of the femtosecond pulses passing through the Fork prism setup at the sample can be expressed as a function of the prism translation Δh as follows:

$$\psi(\omega,\Delta h) = \frac{1}{2}(\Delta h \cdot 368 \ \text{fs}^2/\text{mm}) \cdot (\omega - \omega_0)^2 + \frac{1}{6}(\Delta h \cdot 114 \ \text{fs}^3/\text{mm} - 8000 \ \text{fs}^3)(\omega - \omega_0)^3, \quad (1)$$

where ω_0 is the angular frequency corresponding to 399 nm.

Two-photon photoemission intensity maps were recorded as a function of the applied spectral phase using a 150 cm hemispherical energy analyzer (SPECS Phoibos 150) at an energy resolution set to 20 meV and an angular resolution set to 0.15°. The electrons were collected with a two-dimensional (2D) detection unit consisting of a microchannel plate, a phosphor screen and a charge coupled device camera, delivering energy and angular-resolved 2PPE intensity maps. The detector is able to record in parallel the electron emission at emission angles between $\pm 7°$ without rotation of the sample. For data analysis, 2PPE energy-distribution curves (EDCs) at $k_{\|}$=0 Å^{-1} (normal emission) were extracted from 2PPE intensity maps after normalization and integration over an emission angle regime of $\pm 3°$.

The Cu(111) surface was cleaned by successive sputtering (up to 10 min at 0.5–1.0 kV) and annealing (15 min, 800 K) cycles. The surface quality of the crystal was checked by low-energy electron diffraction and by the two-photon photoemission characteristics (energy and spectral width) of the Shockley surface state (SS) of the Cu(111) surface. For these reference measurements, a different Ti:Sapphire laser system exhibiting a narrow bandwidth emission (FWHM=3 nm at 419 nm, supporting a transform-limited pulse duration of $\tau_{TL} \approx 87$ fs of the SHG light) was used. All 2PPE measurements were performed at room temperature.

B. Cesium adsorption

The adsorption of alkali atoms on metal surfaces has been investigated thoroughly in the past.[23] In the context of the dynamics of charge-transfer processes, cesium adsorption on noble metal surfaces has attracted considerable attention because of the formation of an exceptionally long-lived resonance, first reported for the Cs/Cu(111) system.[6,24–28] The Cs* resonance corresponds to the transient capture of an electron in a 6*s*-6*p* hybrid state by a positively charged Cs$^+$ adsorbate. The excited state decays by electron transfer to the substrate either via a resonant one-electron transfer or via multielectron interactions. The latter process is dominant in the Cs/Cu(111) system.[6,26,27] In the limit of the adsorption of an individual cesium atom on a noble metal, the resonance energy E_{Res} is about 3 eV above the Fermi energy, almost independent of noble metal species and surface orientation.[29–31] With increasing Cs coverage, the resonance energy shifts toward the Fermi energy, a behavior arising from the interaction between the excited Cs* state and the dipole layer formed by the surrounding alkali adsorbates.[26] It is this excited resonance state that is considered in the

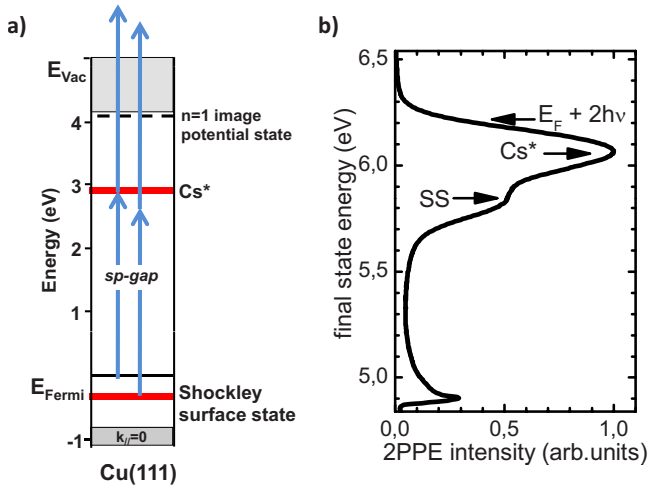

FIG. 2. (Color online) (a) projected electronic structure of Cs/Cu(111) including the relevant 2PPE excitation pathways; (b) EDC, integrated over an emission angle range of ±3° and measured with a phase modulation of GVD=0 fs^2 and TOD=−8000 fs^3. Arrows indicate the positions of the Cs^* peak maximum, the Shockley surface state peak maximum and the high energy cutoff of the 2PPE spectrum at $E_F+2h\nu$.

present study to address details of the adsorbate excitation dynamics using phase modulated laser pulses.

In the experiment the Cs was deposited from a well-degassed (24 h) resistive heated getter source. The total coverage was determined from the change in the low-energy onset of the 2PPE EDC of Cu(111) arising from the change in the surface workfunction induced by the adsorbed Cs.[32] All presented experiments were performed at a Cs coverage of approximately 0.02 ML. The projected surface band structure including the 2PPE excitation pathways relevant for this study is shown in Fig. 2(a). A 2PPE EDC recorded for vanishing GVD of the excitation laser pulse is shown in Fig. 2(b). Two peaks are visible in the EDC. The low-energy peak can be assigned to direct 2PPE from the minimum of the dispersive Shockley surface state band at $k_{\|}=0$ $Å^{-1}$, the high-energy peak is due to photoemission from the excited Cs^* resonance. Note that the position of the Fermi edge at E_F+2 $h\nu$ in the 2PPE spectrum can alter the Cs^* peak shape by cutting off the high-energy tail of the spectrum. We chose a Cs coverage, as seen in Fig. 2(b), for the following reason: The excitation of this surface at 399 nm gives rise to a two peak structure in the EDC, which can be well analyzed and separated by a two-peak fit and which allows an independent analysis of these two different excitation processes. The direct 2PPE from the surface state band bottom and its spectral response to the GVD/TOD phase modulation of the excitation laser pulse has been studied in detail in Refs. 14 and 33. In the present work, we concentrate on photoemission via the transient Cs^* state with emphasis on how the dynamics of the Cs^* intermediate can be revealed by the 2PPE process with a single chirped laser pulse.

III. THEORETICAL MODEL

The present theoretical study is based on a wave-function approach, in which the Cs motion and the exciting laser pulse are treated explicitly. Details about this procedure can be found in Refs. 34 and 35, which treated the effect of the Cs motion on a TR-2PPE signal and photodesorption. We consider three electronic states of the system, the initial electronic state, ϕ_{init,E_i}, of energy E_i, the resonant state localized on the Cs adsorbate, ϕ_{Cs^*} and the final state corresponding to the photoemitted electron at energy E_f, ϕ_{f,E_f}. The time-dependent wave function of the system is then written as

$$|\Psi\rangle = \chi_{init,E_i}(Z,t)|\phi_{init,E_i}\rangle + \chi_{res}(Z,t)|\phi_{Cs^*}\rangle + \int dE_f \chi_{E_f}(Z,t)|\phi_{f,E_f}\rangle. \quad (2)$$

The amplitudes in front of the electronic wave functions depend both on time and on Z, the Cs-surface distance. In the initial state, before the laser pulse, the Cs is in one of the vibrational levels, v, of the Cs-Cu adsorption well centered at Z_{Ads} [energy E_n and wave function $X_v(Z)$]. The above wave function then describes the photoemission from a given electronic initial state and from a given initial vibrational level of the Cs-surface motion into the continuum of photoemitted electrons.

The time-dependent Hamiltonian of the system is written as

$$H(t) = T_Z + H_{el} + \varepsilon(t)D, \quad (3)$$

where T_Z is the kinetic energy operator for the adsorbate motion along the Z coordinate. H_{el} is the electronic part of the Hamiltonian. D is the dipolar operator for the coupling between electronic states induced by the laser field. $\varepsilon(t)$ is the time-dependent laser field. In the present case we use single phase-modulated Gaussian laser pulses as prepared in the experiment using the fork prism pair setup. $\varepsilon(t)$ is calculated from a numerical inverse Fourier transform of the spectral phase modulated laser field $\varepsilon(\omega,\mathrm{GVD},\mathrm{TOD})$ given by

$$\varepsilon(\omega,\mathrm{GVD},\mathrm{TOD}) = \varepsilon_{0,Gauss}(\omega)e^{-i\psi(\omega,\mathrm{GVD},\mathrm{TOD})}. \quad (4)$$

$\varepsilon_{0,Gauss}(\omega)$ is a Gaussian peak of 8.7 nm bandwidth and $\psi(\omega,\mathrm{GVD},\mathrm{TOD})$ is the spectral phase modulation determined from our earlier analysis on the 2PPE of the Cu(111) surface state [see Eq. (1)].[14]

The electronic Hamiltonian H_{el} is represented as a diagonal operator in the basis of the three electronic states defined above

$$H_{el} = [V_0(Z) + E_i]|\phi_{init,E_i}\rangle\langle\phi_{init,E_i}| + \left[V_{res}(Z) - \frac{i}{2}\Gamma_{res}(Z)\right]|\phi_{Cs^*}\rangle\langle\phi_{Cs^*}| + \int dE_f[V_0(Z) + E_f]|\phi_{f,E_f}\rangle\langle\phi_{f,E_f}|, \quad (5)$$

where $V_0(Z)$ is the potential energy curve for the Cs adsorbate in front of the Cu(111) surface. $V_{res}(Z)$ is the potential energy curve for the Cs^* resonant state in front of the surface and $\Gamma_{res}(Z)$ is the decay rate of the Cs^* resonant state. Describing the decay of the excited state by a complex energy is not fully accurate; it may differ at extremely short times[36] and does not properly account for the repopulation of the

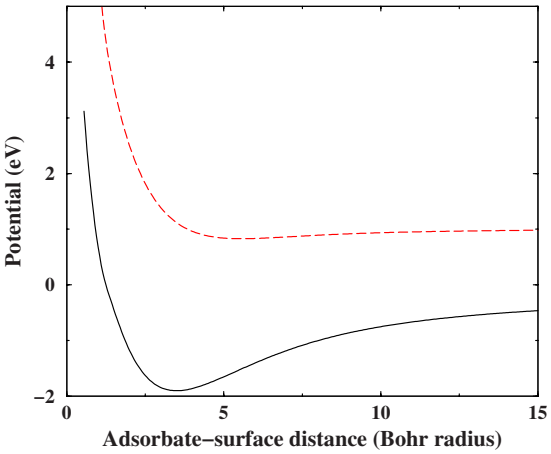

FIG. 3. (Color online) Potential energies used in the present work (adapted from Ref. 35) for Cs adsorbates in front of a Cu(111) surface, as functions of the adsorbate surface distance measured from the surface image reference plane. Full black line: $V_0(Z)$, adsorption potential of the Cs^+ ion, the potential is normalized at zero at infinity. Dashed red line: $V_{res}(Z)$, excited potential energy curve of the Cs^*-Cu(111) system, the excitation corresponds to taking an electron from the Fermi level and bringing it into the lowest unoccupied adsorbate orbital.

ground state.[37] However, the latter point does not play a role here, where only low intensity laser pulses are considered.

The three electronic states depend on Z, the adsorbate-surface distance (see Fig. 3). If we assume that the laser field intensity is weak enough to allow the use of a perturbation treatment, then the excited state amplitudes are given by the following time-dependent coupled equations in the rotating wave approximation:

$$i\frac{\partial \chi_{res}(Z,t)}{\partial t} = \left[T_Z + V_{res}(Z) - \frac{i}{2}\Gamma_{res}(Z)\right]\chi_{res}(Z,t) + \varepsilon(t)\langle\phi_{Cs^*}|D|\phi_{init,E_i}\rangle X_v(Z)e^{-i(E_i+E_v)t}$$

$$i\frac{\partial \chi_{E_f}(Z,t)}{\partial t} = [T_Z + V_0(Z) + E_f]\chi_{E_f}(Z,t) + \varepsilon(t) \times \langle\phi_{f,E_f}|D|\phi_{Cs^*}\rangle\chi_{res}(Z,t). \quad (6)$$

The dipolar couplings between the initial and resonant, and between resonant and final states are supposed to be independent of the initial and final energies and of the adsorbate-surface distance. This simplification in the treatment is linked to the rather limited range of energies that are probed in the studied situation; typically it is in the 200 meV range as given by the width of the Cs^* photoemission peak (see below Fig. 12). Similarly, the range of Cs-surface distances that actually contribute in the present experiment is limited; it is typically given by the spread of the adsorption distances in the initial state and it is not expected to lead to large variation in the dipolar couplings. The Eqs. (6) are then solved by time propagation for a set of initial states (vibrational level v and initial electronic energy E_i). The signal for photoemission of an electron at energy E_f for a given initial state is then given by

$$\text{Signal}(E_i,v;E_f) = \int dZ|\chi_{f,E_f}(Z,T_f)|^2, \quad (7)$$

where T_f is a time long after the laser pulse. The potential energies and width entering in the above equations were taken from our earlier study on the static Cs^*-Cu(111) system.[26,27,34] The present theoretical approach is then parameter-free with the laser pulse shape known from an independent study. The Z dependence of the amplitudes was described on a grid of 1024 points. Typically the number of initial and final states involved in the calculations was in the 30–50 range. The success of our earlier description of two pulse photoemission,[34] in particular, in accounting for the dependence of the TR-2PPE signal on the laser characteristics[38] gives confidence in the present approach and in the Cs/Cu(111) data to represent the dynamics of the system.

The energy spectrum of emitted electrons for a given experimental situation can be obtained from Eq. (7) by summing incoherently the contributions from the various possible initial states

$$Sp(E_f) = \int dE_i \sum_v P_v(T)\ \text{Signal}(E_i,v;E_f). \quad (8)$$

The initial vibrational level population, $P_v(T)$, is given by the substrate temperature T. In the results shown below we assumed that the initial electronic state belongs to a broad band, i.e., that the initial electronic state that is resonantly coupled with the Cs^* state at Z_{Ads} at the laser central frequency ω_0 is not close to the edge of a band. The sum over E_i is then taken symmetrically around this resonance condition. Actually, in the present case, only the cutoff at the Fermi energy plays a role in this integration. One can stress that in the case where the Cs^* state is resonantly coupled at the laser central frequency ω_0 with the bottom of the surface state, the above summation over initial states would be asymmetric and would only contain terms above the resonance condition. The present theoretical study only includes photoemission through the Cs^* state, it does not include direct two-photon photoemission from the surface state and thus, it only describes the peak labeled Cs^* in Fig. 2. Two features in the computed and experimental energy spectrum $Sp(\varepsilon)$ are determined: the position of the maximum and the full width at half maximum of the spectrum. These are discussed in more detail below.

One can stress the characteristics of the present approach, based on a wave-function representation. It does not incorporate completely the effect of the interaction of the system with the thermal bath of bulk electrons. In particular, it does not include the so-called pure dephasing process (coherence decay without population decay induced by the interaction with the electron bath) that is usually introduced phenomenologically via a T_2^* time in TR-2PPE modeling using, e.g., Bloch optical equations.[3] However, as discussed in Ref. 34, there are several sources of pure dephasing in this system and two very efficient sources are taken into account in the

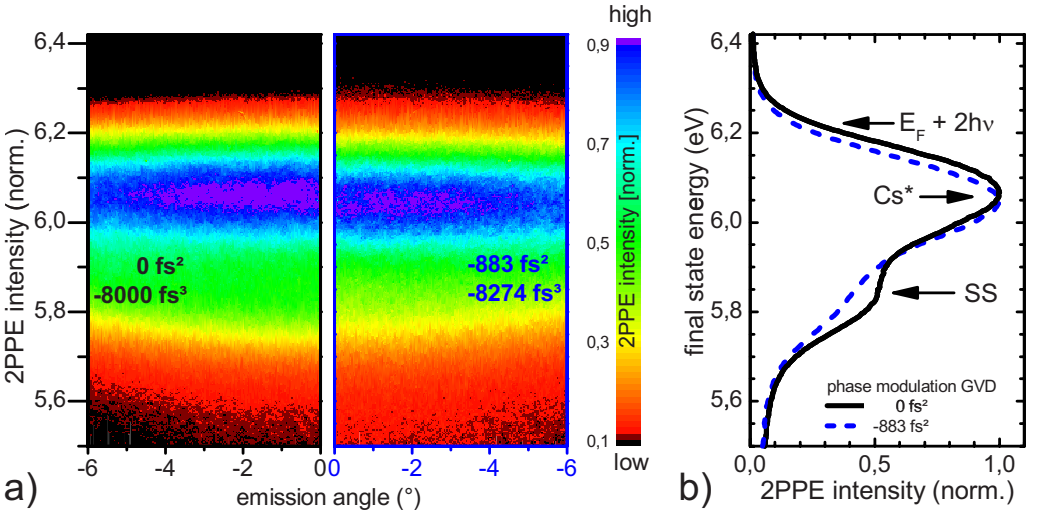

FIG. 4. (Color online) CP-2PPE data recorded at GVD=0 fs^2 (TOD=−8000 fs^3) and at GVD=−883 fs^2 (TOD=−8274 fs^3); (a) comparison of two 2PPE $E(k_{\|})$ intensity maps for two different chirp parameters (left: GVD=0 fs^2, right: GVD=−883 fs^2); the 2PPE yield increases from red via green to blue. The nondispersing intensity maximum at about 6.05 eV is due to the photoemission from the Cs^* resonance state. (b) electron distribution curves for GVD=0 fs^2 (black line) and GVD=−883 fs^2 (broken blue line) as deduced by angular integration of the intensity map between −3° and +3° emission angle; clear energy shifts of the Shockley SS peak and of the Cs^* resonance peak are observed as the GVD of the excitation pulses decrease to a value of −883 fs^2. For clarity, the data have been normalized to the Cs^* peak intensity maximum.

present approach. The summation over the complete set of possible initial states as well as the time dependence of the Cs^* state energy because of the adsorbate motion introduce a loss of coherence in the system which was actually found to account for the dephasing experimentally observed in this system (see discussion in Ref. 34). Though we cannot rule out a dephasing effect because of the Cs^* interaction with the surface thermal bath since we did not evaluate it, we can infer from the results in Ref. 34 that it is not dominating the coherence decay in this system, giving confidence in the present approach.

IV. RESULTS AND DISCUSSION

In the following main section of this paper we will start with a presentation of the experimental chirped pulse data of the Cs/Cu(111) system with an emphasis on the changes in peak energy and peak width of the Cs^* resonance in the 2PPE spectrum as function of the applied GVD. These data will then be interpreted by a comparison with our model calculations under consideration of Cs^* resonance lifetime and Cs nucleus motion. Within the calculation it is possible to selectively activate and deactivate the different processes involved in the complex adsorbate excitation process. This enables us to identify the relevant mechanisms responsible for the observed changes in the experimental traces. The impact of the adsorbate dynamics on peak energy and on peak width will be addressed separately.

1. Chirped pulse 2PPE experimental data of Cs/Cu(111)

Figure 4 compares 2PPE data of Cs/Cu(111) recorded with 399 nm light pulses exhibiting a vanishing GVD (TOD=−8000 fs^3) and 2PPE data recorded with GVD =−883 fs^2 (TOD=−8274 fs^3). In the 2PPE intensity maps [Fig. 4(a)] the nondispersing contribution from the Cs^* resonance at a final state energy of about 6.05 eV as well as the upward dispersing contribution from the Shockley surface state at the bottom of the color-coded intensity band are clearly resolved. For better comparison, the two intensity maps were normalized to the Cs^* peak maximum intensity. Clear differences are observed, demonstrating the sensitivity of the 2PPE spectrum to the chirp of the excitation pulse. The corresponding EDC at $k_{\|}=0$ $Å^{-1}$ shown in Fig. 4(b) underscore the distinct effect caused by the modulation of the spectral phase on the 2PPE process. The Cs^* photoemission peak undergoes a downward shift in energy in response to the negative GVD/TOD and its width also slightly narrows. In contrast to this, the direct 2PPE from the surface state is reduced in amplitude with respect to the Cs^* resonance, broadens and exhibits an upward shift in energy. In effect, the SS peak becomes much less visible in the flank of the Cs^* peak.

Next we will present results of the quantitative analysis of this chirp dependence in the 2PPE spectral response. The two main quantities that will be considered are the Cs^* peak position X_{Cs} and the Cs^* peak width full width at half maximum, $FWHM_{Cs}$, in the 2PPE spectra as a function of the spectral phase applied to the femtosecond laser pulses. We performed two-peak fits to the 2PPE EDCs consisting of a Lorentzian (peak amplitude A_{SS}, peak position X_{SS}, and peak width $FWHM_{SS}$) to account for a homogeneously (lifetime-) broadened surface state peak,[39] and a Gaussian (A_{Cs}, X_{Cs}, and $FWHM_{Cs}$) for the Cs^* peak, which, at room temperature, is strongly inhomogeneously broadened due to vibrational excitations.[40,41] To avoid distortions of the fit because of the interference of the Cs^* photoemission peak with the Fermi energy cutoff at the high-energy part of the spectrum [see

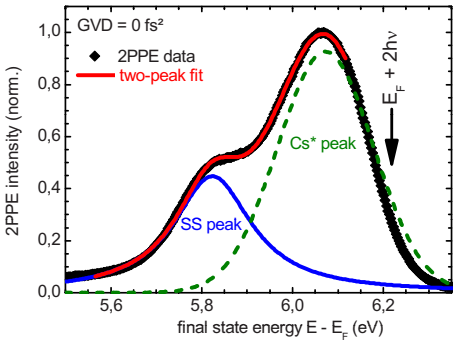

FIG. 5. (Color online) Result of the two-peak fit (solid grey/red line) in comparison to the experimental EDC ($k_{\|}$=0 Å^{-1}) at GVD =0 fs^2 (TOD=−8000 fs^3) (black diamonds). The fitting range was restricted to energy values between 5.57 and 6.12 eV to avoid distortions due to the influence of the Fermi energy distribution at the high-energy cutoff of the spectrum (see arrow).

marker in Fig. 4(b)] the fitting range was restricted to energy values between 5.57 and 6.12 eV. In Fig. 5, the result of the fit is compared to the experimental data for the zero-GVD case.

Chirp dependencies of SS peak energy and SS peak width have been reported before for the pristine Cu(111) surface.[14,33] The data from our survey[14] have been used to constrain the number of fitting parameters and to check the quality of the fitting results, respectively. The relative shift of the SS peak energy X_{SS} as function of the applied GVD has been directly adopted from a pristine Cu(111) data set measured prior to the Cs/Cu(111) data set (published in Ref. 14) and has been fixed for the fitting procedure. Only a slight, GVD-independent correction in the SS peak energy X_{SS} by +4 meV in comparison to the pristine Cu(111) data was necessary to account for the binding energy shift of the Shockley surface state arising from the interaction with the Cs adsorbate.[42]

The chirp dependence in the peak width FWHM$_{SS}$ of the surface state was left as a free fitting parameter, however, the results of the fits were directly compared with the chirp dependence for the pristine Cu(111). Figure 6 compares the peak width of the pristine Cu(111) surface and the Cs-covered surface. It is evident that the two-peak fits applied to the Cs/Cu(111) data deliver FWHM$_{SS}$ values which reproduce the chirp dependence observed for the pristine Cu(111) surface strikingly well. Only an overall broadening of the Cs/Cu(111) data by 42 meV is observed, which arises from the interaction between the surface state and the adsorbed Cs adatoms.[28] In summary, the high consistency between the two data sets regarding the Shockley surface state peak parameters shows that the surface state chirp evolution is, if at all, affected only marginally by the presence of the Cs adsorbate.

Next, we will consider in detail the results for the Cs peak shift X_{Cs} and the Cs peak width FWHM$_{Cs}$. The chirp dependencies of the two parameters are shown in Fig. 7. Overall, a maximum shift in the peak position X_{Cs} of 30 meV within the probed GVD regime is observed. In comparison to the surface state data, the X_{Cs} trace does not show a local minimum at negative GVD values. Instead, the Cs peak position

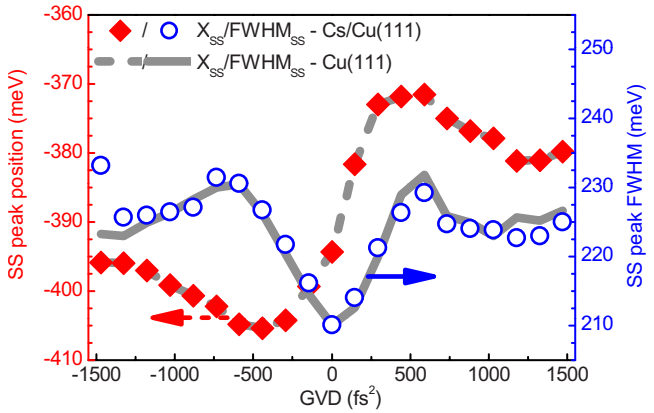

FIG. 6. (Color online) Peak position X_{SS} and peak width FWHM$_{SS}$ of the Shockley Surface state for the pristine Cu(111) surface (dashed gray line/full gray line) and the Cs covered surface (filled red diamonds/open blue circles) as deduced from the fitting procedure in this work. The FWHM$_{SS}$ value of the pristine Cu(111) surface have been shifted by 42 meV to larger values to account for the lifetime broadening of the Shockley surface state in Cs/Cu(111) due to the interaction with the Cs adsorbates.

stabilizes for GVD values smaller than −750 fs^2. On the other hand, a local maximum at positive GVD values is present in the Cs data so that the X_{Cs} trace does not exhibit an antisymmetric chirp dependence as observed for the SS peak shift. For the Cs-peak width FWHM$_{Cs}$ we also observe a chirp dependence which significantly differs from the FWHM$_{SS}$ trace (see Fig. 6). The maximum change in the FWHM$_{Cs}$ due to the chirp variation is only 10 meV. The overall behavior of the curve is essentially inverted in comparison to the SS data so that at vanishing GVD, the Cs peak width is maximum. Note also the lack of local extrema at finite positive and negative GVD values which are present at ±700 fs^2 in the case of the SS data. The FWHM$_{Cs}$ curve seems to show also a slight asymmetric character exhibiting a steeper slope at positive GVD values.

Also Petek *et al.*[13] have published data sets for a similar experiment on Cs/Cu(111) before, covering a more restricted

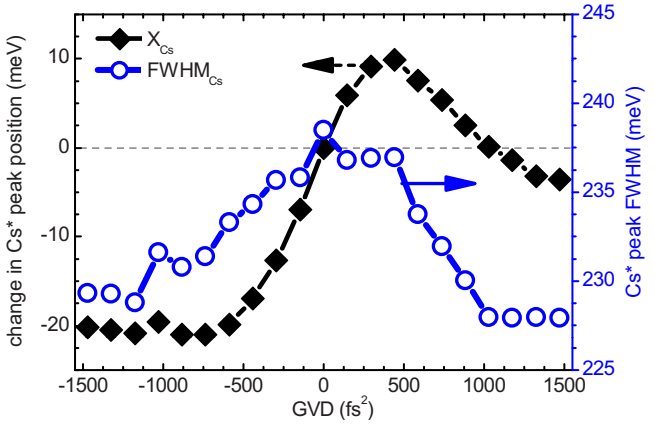

FIG. 7. (Color online) Cs* peak position X_{Cs} (black diamonds) and peak width FWHM$_{Cs}$ (open dots) as function of the applied GVD. The peak position X_{Cs} exhibits a clear asymmetry with respect to chirp and the peak width FWHM$_{Cs}$ maximizes for a vanishing chirp.

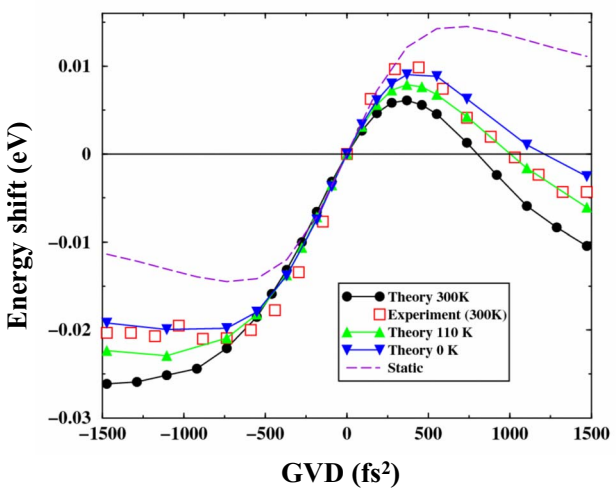

FIG. 8. (Color online) Calculated Cs* peak traces as a function of the applied chirp for different temperatures in comparison to experimental room temperature data from this work; the black line/full dots show the results of room temperature calculations, which take the full dynamics of the Cs adsorbate into account, including the nucleus motion induced by the excitation. The purple dashed line shows theoretical data for the static case, i.e., no nucleus motion. The energy scale is referred to the peak position for zero GVD.

GVD regime. Our experimental results match the results reported in that work qualitatively.

In a recent publication we have shown that the chirp dependencies of the surface state peak position and peak width exclusively map the time and phase characteristics of the excitation laser pulse.[14] A main aspect of the data interpretation was the instantaneous nature of the excitation pathway in the 2PPE process from the surface state of pristine Cu(111). The clear deviations in the Cs data in comparison to the surface state data indicate that, next to the laser pulse characteristics, the Cs chirp traces also comprise information on the dynamics of the Cs* state that is transiently populated in the 2PPE process. In the following we will directly compare our experimental data to theoretical data based on the approach described in Sec. III. This comparison enables us to go deeper into the analysis of the physical phenomena underlying the chirp dependence. In this way, we will decipher how chirped pulse measurements can unveil the dynamics of the excited adsorbate during the 2PPE process.

2. *Impact of Cs dynamics on chirped pulse 2PPE: Interpretation under consideration of model calculations*

Cs* *peak position*. Figure 8 compares calculated Cs* peak position traces with the experimental data of this work. Shown are theoretical room temperature results under consideration of the full nucleus motion of the Cs adsorbate as induced by the laser excitation (black full line/full dots) as well as for the so-called "static" case, i.e., with the Cs atom fixed at its equilibrium adsorption distance Z_{Ads} (purple dashed line). The Cs* peak position for vanishing GVD depends on the laser pulse length as well as on the surface temperature. In order to stress the chirp effect and to allow for an easier comparison between experimental and theoretical results, only the displacement of the peak position relative to its position for a vanishing chirp is presented and we only briefly discuss the absolute position at GVD=0 fs^2, which we did not study in detail.

In the static calculation, the photoemission peak at GVD =0 fs^2 is maximum at the resonance position at the adsorbate equilibrium position, i.e., at an energy equal to the sum of the Cs* energy (at Z_{Ads}) and of the photon energy. In the full calculations, the peak at GVD=0 fs^2 is slightly below the resonance position (from 10.2 meV at 0 K to 23.6 meV at 300 K). There are two reasons for this downshift: first the Cs* motion between the two photoabsorptions and second the asymmetric spread of the Cs vibrational wave function in the adsorption well that favors large Z. Because of the first effect, the energy shift at GVD=0 fs^2 depends strongly on the laser pulse shape.

We start by discussing the theoretical results obtained for the static case (no nucleus motion considered). The overall trend predicted in this case from our calculations is the following: positive GVD leads to an upward shift of the peak and vice versa. Furthermore, clear local extrema in the peak position appear on both sides of zero GVD. The peak position trace exhibits an almost antisymmetric shape with respect to the chirp variation. Actually, the peak position is not exactly antisymmetric with respect to GVD, due to the presence of TOD: reversing the sign of the GVD does not affect the sign of the TOD, so that a perfect antisymmetry cannot be reached. The calculated variation in the peak position with the chirp is similar to that observed experimentally for the surface state peak (see Fig. 6) and different from that experimentally observed for the Cs* peak (see Fig. 7). One can stress that in both cases (surface state peak and static calculation), the system is not evolving during the 2PPE process; the difference lies in the existence of a long-lived intermediate state in the present "static" study compared to the direct 2PPE from the surface state.

When the excitation induced Cs motion is taken into account, the chirp-dependence of the calculated Cs* peak position changes significantly. In comparison to the static case the peak maximum is systematically lower in energy, an effect which is stronger for large negative or positive GVD. Even more, the antisymmetric character disappears and the calculated behavior is very close to the experimental Cs* data. Inclusion of the Cs motion thus catches a large part of the relevant physics responsible for the chirp dependence of the Cs* peak position, or from another point of view, the difference between the 'static' and 'full' calculations unveils the evolution of the Cs* state during the 2PPE process. One can notice that the effect of the Cs motion (difference between the static and full calculations) amounts to 15–20 meV; this is a sizeable effect, non-negligible compared to the photoemission peak width at 300 K (in the 240 meV range). It is thus easy to evidence the Cs motion in a single-pulse experimental scheme even at 300 K when thermal broadening is large. Figure 8 also presents results from the full calculation at three different surface temperatures: 0, 110, and 330 K. The shape of the variation of the peak position is the same with only a limited T variation: it appears that the deviation from the static results, i.e., the effect of the Cs adsorbate motion increases when the surface temperature in-

creases (this is essentially the effect of the initial vibrational temperature of the adsorbate).

Former works have indeed shown that populating the Cs^* state induces a motion of the Cs adsorbate away from the surface and, because of the shape of the potential energy surfaces (see Fig. 3), this leads to a downward shift in Cs^* peak energy in the photoemission spectrum (see discussions, e.g., in Refs. 34, 43, and 44). Here, the downward shift at GVD=0 fs^2 in the full calculation compared to the static calculation comes from this effect. The calculations show furthermore that the application of GVD (positive or negative) to the pulses results in an additional downward shift of the Cs^* peak.

The modulation of a laser pulse by GVD gives rise to a frequency drift (chirp), but also to an increase of the pulse length. To characterize the link between the various characteristics of the chirped pulse and the downward shift in energy, we performed model calculations using unchirped laser pulses of different pulse lengths.

For this purpose, we used a time-dependent Gaussian laser field that describes a GVD-only modulation, (i.e., no TOD spectral phase modulation), in which the frequency drift term has been removed

$$\varepsilon(t) = \frac{A}{\sqrt[4]{1+w^2}} \exp\left[-\frac{2\,\mathrm{Log}(2)}{1+w^2}\frac{t^2}{\tau_{TL}^2}\right]\cos(\omega_0 t). \qquad (9)$$

The pulse duration parameter was set to a value of τ_{TL} =20 *fs*. *w* is the bandwidth-dependent chirp parameter, which, however, is exclusively used to adjust the overall pulse length. *w* is related in this case to the GVD in fs^2 by

$$\mathrm{GVD} = \frac{\tau_{TL}^2}{4\ln 2} w = 144.3\ \mathrm{fs}^2\, w \qquad (10)$$

In parallel, we also made calculations with "usual," chirped Gaussian pulses (TOD=0 fs^3) with the same *w* parameter and we compared the results obtained with these two sets of pulses. In this way we can separate the effect of the frequency drift from that of the pulse lengthening in the chirped pulses. The peak shifts as function of the pulse length were calculated for *T*=0 K (the Cs adsorbate is initially in the ν =0 vibrational level) and are shown in Fig. 9 (full line with green open circles), together with the calculated chirped Gaussian pulse results without Cs motion ("static" calculation, dashed black line) and with Cs motion (red line with full circles). Note that the shortest pulses are obtained for vanishing GVD (w=0 fs^2) and the longest for maximum positive and minimum negative GVD values. The pure increase in the pulse length (green line), without any phase modulation, already gives rise to a significant downward shift of the Cs^* peak position. The interpretation is the following: For a longer single laser pulse, the time delay between the absorption of the two photons of the 2PPE process can be larger allowing to probe the Cs motion from the surface over a longer time span and leading to a further decrease of the Cs^* peak energy. At very large chirp parameter, either positive or negative, the pulse length becomes very large and can be much longer than the intermediate state lifetime, leading to the saturation of the above effect. This accounts for the stabilization of the shift of the peak maximum at large $|w|$.

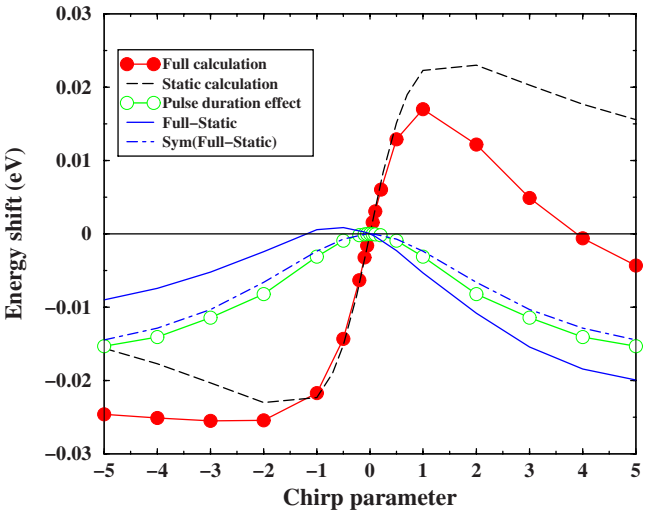

FIG. 9. (Color online) The full green line/open dots show the Cs^* peak position as function of the pulse length in units of the chirp parameter w for laser pulses without phase modulation where the effect of the Cs motion is included. For comparison calculations with phase modulated pulses of the same duration have been added; dashed black line: static calculation; red line/full circles: calculation with Cs motion. All calculations were performed at *T*=0 K and without TOD. For the sake of discussion, the full blue line shows the difference between the full calculation and the static calculation whereas the dashed-dotted blue line shows this same difference averaged over positive and negative GVD.

Figure 9 also presents the difference between the full and the static calculation results as a function of the GVD (full blue line) as well as this difference averaged over positive and negative GVD (dashed-dotted blue line). One can see that the downshift observed in the long-pulse calculations (only pulse length effect) is on the order of the difference between the static and the full calculations for the chirped Gaussian pulses and furthermore almost equal to this difference when positive and negative GVD are averaged. We can then conclude that the departure from the antisymmetric shape observed in the full calculations with chirped pulses is mainly a consequence of the increase of the pulse length and not so much of the frequency drift inside the chirped pulse. The effect of the frequency drift inside the pulse obviously only plays a minor role in revealing the effect of the adsorbate motion on the Cs^* peak position in the photoemission electron spectrum, it is responsible for the small difference between the green line and the full blue line, it roughly changes sign with the GVD, depending on whether the frequency drift and the Cs^* energy change induced by the motion are in the same or in opposite directions.

Furthermore, we evaluated the effect of the Cs^* resonance lifetime on the chirped pulse Cs^* peak curve. The resonance lifetime provides the effective probing window for the 2PPE process and it should, therefore, govern the sensitivity of the experiment to the nucleus motion. Calculations were performed with the Cs^* decay rate $\Gamma_{res}(Z)$ multiplied by a constant factor (0.5, 2.0, and 5.0). The results are summarized in Fig. 10(a). The shape of the peak curve exhibits a clear dependence on the resonance lifetime. Particularly the devia-

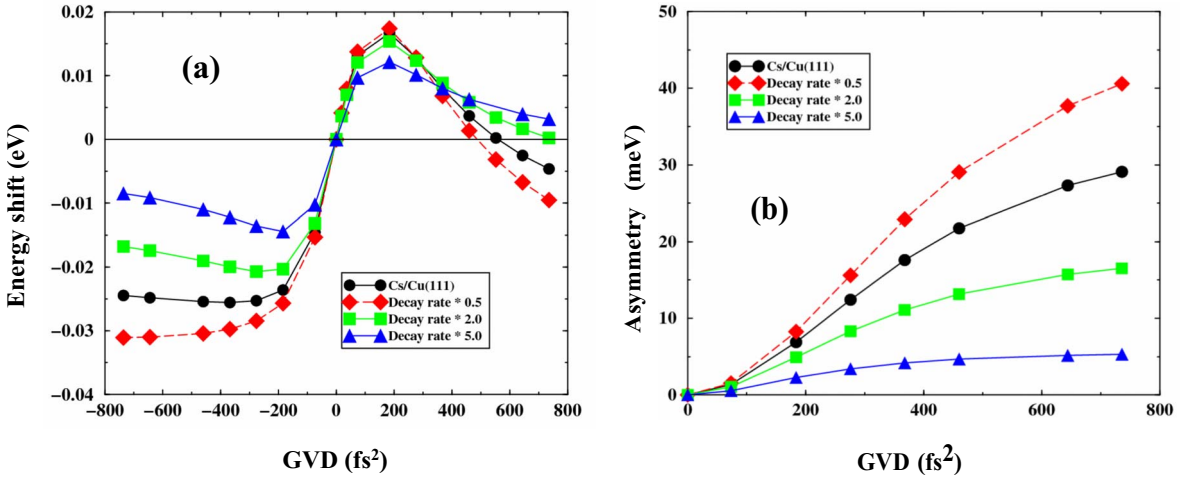

FIG. 10. (Color online) (a) Calculated energy shift of the Cs* peak position as a function of the chirp parameter for the Cs/Cu(111) system and the model systems with a variable decay rate. In all cases, the vibrational temperature is 0 K, the effect of the electronic Fermi edge is not included. The energy shift is plotted relative to its position for an unchirped pulse (pure Gaussian 20 fs); (b) Asymmetry of the chirp effect on the Cs* peak position of emitted electrons in Cs/Cu(111) and model systems as defined by Eq. (11). The surface temperature is 0 K and no Fermi edge effect is taken into account.

tion from the antisymmetric shape of the curve that we associate with the adsorbate motion becomes more pronounced as the resonance lifetime increases. What is the minimum resonance lifetime at which the Cs motion in front of the surface can still be probed within a chirped-pulse 2PPE experiment? For an estimate we calculated for each curve in Fig. 10(a) the asymmetry parameter A defined as

$$A(\mathrm{GVD}) = 2 \cdot \Delta X_{Cs}(0, \mathrm{TOD}_0) - \Delta X_{Cs}(\mathrm{GVD}, \mathrm{TOD}_{pos}) - \Delta X_{Cs}(-\mathrm{GVD}, \mathrm{TOD}_{neg}). \quad (11)$$

Figure 10(b) compares the asymmetry parameter for different lifetimes as function of the applied GVD ($T=0$ K). For the shortest lifetime (on the order of 6 fs at the adsorbate equilibrium position), a residual asymmetry of about 5 meV is still visible for large GVD values. At the given resonance linewidth of about 300 meV at room temperature such a small value is of course a challenge for a 2PPE experiment but not impossible to detect.[45]

To summarize this section: We find a quantitatively satisfying agreement in the Cs* peak position between theoretical calculations and experimental data. We show that the chirped pulse 2PPE traces contain information on the dynamics of the Cs* motion away from the surface induced by the photoexcitation. The signature of the Cs motion mainly arises from the change in the laser pulse length due to the applied phase modulation, probing the adsorbate motion on successive longer time scales. In a way, in this single-pulse scheme, the change in pulse length provides the clock that probes the adsorbate dynamics as a function of time. In the following we will now compare the experimentally determined chirp dependence in the Cs* peak width (FWHM) with the results of the theoretical calculations.

Cs* *peak width*. Figure 11 presents the calculated variation in the Cs* FWHM as a function of the GVD parameter for a surface temperature of $T=0$ K. Note that these results come from the same calculations with 20 fs chirped Gaussian pulses that have been presented in Fig. 9. The data includes all the broadening effects for a 0 K system with a vanishingly small Cs surface density, except for the contribution from the experimental electron energy analyzer (see a discussion of the various causes of broadening in Ref. 41). Three sets of results are shown: the full calculation including Cs motion (full red dots), the result for the static case (dashed line), and the calculation without phase modulation, but with the pulse length effect and the Cs motion [open green dots, laser shape given by Eq. (9)]. In the entire GVD regime, the FWHM in the static calculation is found to be smaller than in

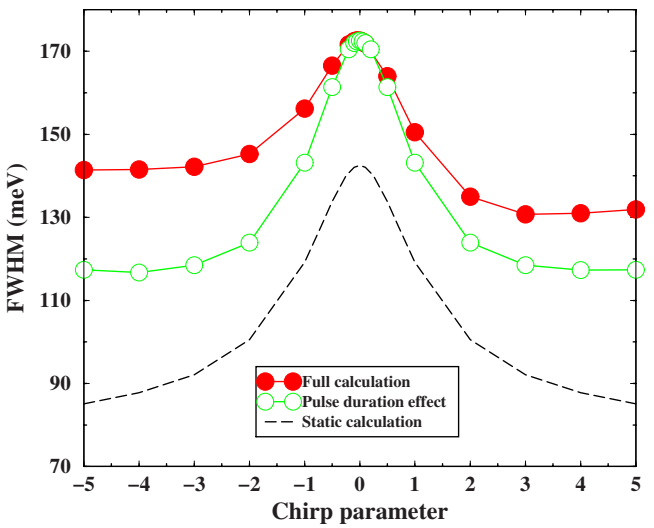

FIG. 11. (Color online) calculated Cs* FWHM as a function of the GVD parameter at $T=0$ K. Note that TOD was not included in these calculations, at vanishing GVD the pulse duration is 20 fs. Dashed line: static case (no Cs motion); full red dots: full calculation including Cs motion; open green dots: effect of the pulse length increase alone, i.e., no phase modulation is applied to the excitation pulse.

the full calculation. The difference is due to the spread of adsorption distance Z_{Ads} in the $\nu=0$ vibrational level of the Cs-surface system that is obviously absent in the static calculation. Actually, the static result at $w=0$ is dominated by the finite laser band width.

The value of 172 meV at 0 K for the full calculation at $w=0$ is very close to the experimental result of about 180 meV reported by Petek *et al.*[13] Actually, test calculations with a Gaussian pulse of 19 fs, a vanishing GVD and a surface temperature of 33 K, closer to the experimental conditions in Ref. 13 yield a peak width of 184 meV.

In the three calculations, the FWHM is maximum for GVD≈ 0 fs^2 (note that the maximum of the FWHM occurs for a slightly negative chirp parameter in the full calculation) and monotonically decreases with increasing GVD and/or pulse length. The amplitude in the FWHM change induced by the pulse length variation only (open green dots) is comparable or even larger than for the full calculation trace (full red dots). We therefore conclude that the overall decrease in the peak FWHM in the full calculation is to a large part because of the increase in the pulse length. We can therefore stress that this contribution to the FWHM dependence reflects a property of the laser pulse and is not linked to the dynamics of the adsorbate excitation. The FWHM asymmetry in the full calculation arises, however, from the interplay between the frequency shift due to the GVD and the Cs motion. The interpretation is the following: When the Cs* state is excited, the Cs adsorbate starts to move out and the Cs* energy decreases leading to a downshift of the Cs* peak position and at the same time to a broadening of the detected photo-emission peak. If the pulse exhibits a positive GVD, the change in laser frequency with time is opposite to that of the Cs* energy shift and they can partly compensate each other, thus decreasing the photoemission peak broadening. If a negative GVD is applied, both effects are in the same direction leading to a broadening of the photoemission peak. This control of peak FWHM by the sign of the GVD is, however, limited. Indeed, the laser frequency drift is linear in time and can therefore only partly compensate the energy variation of the Cs* state which is expected to vary quadratically with time. This shows that, in contrast to the Cs* peak position calculations, the frequency drift plays a much more significant role for the peak FWHM dependence.

Figure 12 presents a comparison between experimental (full dots) and theoretical (open squares) FWHM data for the Cs/Cu(111) system at 300 K. In this case, we used the experimentally determined pulse parameters for a full calculation that includes GVD and TOD. The increase in temperature gives rise to a large overall broadening of the Cs* peak in comparison to the $T=0$ K calculation, as expected (see a discussion in Ref. 41). The calculated value of about 237.5 meV at GVD$=0$ fs^2 matches the experimental value of 238 meV once again rather well. The calculated FWHM at 300 K is minimum for a small positive GVD, in contrast to the above results at 0 K in the absence of TOD which maximize in the region of vanishing GVD. The small asymmetry between positive and negative GVD already seen at 0 K and attributed to the interplay between frequency drift and Cs* motion is still present at 300 K.

The behavior of the theoretical FWHM at 300 K is different from the one observed experimentally, which exhibits a maximum for vanishing GVD. However, one can stress the rather small overall variation of the 300 K FWHM: in both cases, it only amounts to a few per cent, much less than found at 0 K in the absence of TOD. This can be attributed to the very large broadening introduced by the thermal distribution of Cs adsorption distances in the initial state (see a discussion in Ref. 41). This broadening dominates and tends to hide all the other broadening contributions and their possible chirp dependence. The origin of the discrepancy between theoretical and experimental FWHM variation at 300 K is unclear, especially in view of the agreement found for the peak position. Indeed the linewidth is expected to be more sensitive to the details of the shape and the chirp of the laser pulse than the position of the peak maximum. Beside possible inaccuracies in the experimental and theoretical procedures, the sensitivity of the FWHM to the actual laser temporal variation as well as the interplay between this variation and the Cs adsorbate motion, as demonstrated in Fig. 11, might explain the present difference.

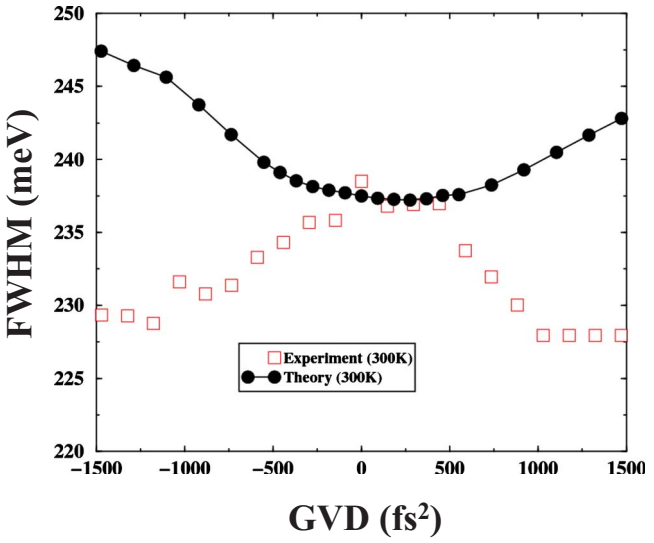

FIG. 12. (Color online) Cs* peak FWHM as a function of the experimentally applied GVD and TOD phase modulations (pulse parameters: $\tau_{TL}=26,9$ *fs*, $\mathrm{TOD}_0=-8000$ *fs*^{3}) at $T=300$ K; full dots: full calculation including Cs motion; open squares: experimental data.

V. SUMMARY AND CONCLUSION

We performed a combined experimental and theoretical study on the effect of phase-modulated (chirped) pulses on the 2PPE spectra of Cs/Cu(111). The present work extends an earlier work by Petek *et al.*;[13] in particular, we were able to analyze much further the phenomena underlying the 2PPE process in a single-pulse scheme using chirped laser pulses and show how it can reveal the evolution of the adsorbate system during the photoemission. We quantitatively prove that the position and width of the Cs* photoemission peak as a function of the applied chirp are directly related to the dynamics of the adsorbate motion away from the surface that is triggered by the laser-induced excitation: the excited Cs* adsorbate moves between the absorption of the two photons

of the 2PPE process. In a time-resolved experiment, the two photons originate from two different pulses with a variable controlled time delay between them, thus probing the evolution of the system between the two pulses. In the present single-pulse scheme experiment, the two photons belong to the same pulse and the Cs evolution is revealed by the variation (chirp) of the laser characteristics during the pulse. One can stress that two characteristics of the chirped pulse are responsible for the observed chirp dependence: the change of pulse duration and the frequency drift. In particular, we showed that the energy shift of the photoemission peak maximum can be attributed dominantly to a pulse duration effect. It appears that the adsorbate motion is easier to evidence on the photoemission peak position rather than on the FWHM, at least at room temperature.

Thus, spectroscopy with chirped, i.e., phase-modulated, pulses can provide insights into the ultrafast dynamics of adsorbates and comparison to theoretical data can make a quantitative analysis possible. Chirped-pulsed nonlinear spectroscopy may therefore be a useful tool to complement pure time-domain (pump-probe) experiments. We particularly expect that for a given spectral bandwidth of the laser pulse the chirped-pulse technique can exceed the time resolution of a pump-probe experiment since it provides an intrapulse probe. The possibility to observe the Cs^* adsorbate motion at room temperature, despite the very large thermal broadening of the photoemission peak, supports this. Model systems which could prove the potential sensitivity of CP-2PPE to ultrafast surface process are for instance the small alkalis (Na, Li) adsorbed on noble metal surfaces, which exhibit much shorter resonance lifetimes than the Cs adsorbate chosen for the present study. Corresponding studies are under progress.

ACKNOWLEDGMENTS

We thank Andreas Ruffing and Frederik Deicke for experimental support. This work was supported by the Research Center OPTIMAS and the Deutsche Forschungsgemeinschaft through DFG GRK 792 "Nichtlineare Optik und Ultrakurzzeitphysik."

*Corresponding author.
†bauer@physik.uni-kiel.de
‡jean-pierre.gauyacq@u-psud.fr

[1] J. W. Gadzuk, Chem. Phys. **251**, 87 (2000); J. P. Gauyacq, A. G. Borisov, G. Raseev, and K. Kazansky, Faraday Discuss. **117**, 15 (2000).
[2] T. Fauster and W. Steinmann, in *Photonic Probes of Surfaces*, Electromagnetic Waves: Recent Developments in Research Vol. 2, edited by P. Halevi, (North-Holland, Amsterdam, 1995), p. 347.
[3] H. Petek and S. Ogawa, Prog. Surf. Sci. **56**, 239 (1997).
[4] M. Bauer and M. Aeschlimann, J. Electr. Spec. **124**, 225 (2002).
[5] T. Fauster, M. Weinelt, and U. Höfer, Prog. Surf. Sci. **82**, 224 (2007).
[6] J. P. Gauyacq, A. G. Borisov, and M. Bauer, Prog. Surf. Sci. **82**, 244 (2007).
[7] S. D. Kevan, Phys. Rev. Lett. **50**, 526 (1983).
[8] K. Boger, M. Weinelt, and T. Fauster, Phys. Rev. Lett. **92**, 126803 (2004).
[9] A. G. Borisov, A. K. Kazansky, and J. P. Gauyacq, Surf. Sci. **526**, 72 (2003).
[10] A. Hotzel, K. Ishioka, E. Knoesel, and G. Ertl, Chem. Phys. Lett. **285**, 271 (1998).
[11] C. Reuß, I. L. Shumay, U. Thomann, M. Kutschera, M. Weinelt, Th. Fauster, and U. Höfer, Phys. Rev. Lett. **82**, 153 (1999).
[12] A. D. Miller, I. Bezel, K. J. Gaffney, S. Garrett-Roe, S. H. Liu, P. Szymanski, and C. B. Harris, Science **297**, 5584 (2002).
[13] H. Petek, H. Nagano, M. J. Weida, and S. Ogawa, J. Phys. Chem. A **104**, 10234 (2000).
[14] F. Steeb, S. Mathias, A. Fischer, M. Wiesenmayer, M. Aeschlimann, and M. Bauer, New J. Phys. **11**, 013016 (2009).
[15] The term "chirp" used throughout this paper denotes a general phase modulation.
[16] R. L. Fork, O. E. Martinez, and J. P. Gordon, Opt. Lett. **9**, 150 (1984).
[17] O. E. Martinez, J. P. Gordon, and R. L. Fork, J. Opt. Soc. Am. A **1**, 1003 (1984).
[18] R. L. Fork, C. H. Brito Cruz, P. C. Becker, and C. V. Shank, Opt. Lett. **12**, 483 (1987).
[19] W. Sellmeier, Ann. Phys. Chem. **219**, 272 (1871).
[20] Heraeus Quarzglas Datasheet "Quarzglas für die Optik, Daten und Eigenschaften" (2007).
[21] R. E. Sherriff, J. Opt. Soc. Am. B **15**, 1224 (1998).
[22] D. Marcuse, Appl. Opt. **19**, 1653 (1980).
[23] For an overview on this topic, see, for instance, *Physics and Chemistry of Alkali Adsorption*, edited by H. P. Bonzel, A. M. Bradshaw, and G. Ertl (Elsevier, New York, 1989).
[24] M. Bauer, S. Pawlik, and M. Aeschlimann, Phys. Rev. B **55**, 10040 (1997).
[25] S. Ogawa, H. Nagano, and H. Petek, Phys. Rev. Lett. **82**, 1931 (1999).
[26] A. G. Borisov, A. K. Kazansky, and J. P. Gauyacq, Surf. Sci. **430**, 165 (1999).
[27] A. G. Borisov, J. P. Gauyacq, A. K. Kazansky, E. V. Chulkov, V. M. Silkin, and P. M. Echenique, Phys. Rev. Lett. **86**, 488 (2001).
[28] M. Wiesenmayer, M. Bauer, S. Mathias, M. Wessendorf, E. V. Chulkov, V. M. Silkin, A. G. Borisov, J.-P. Gauyacq, P. M. Echenique, and M. Aeschlimann, Phys. Rev. B **78**, 245410 (2008).
[29] H. Petek, H. Nagano, M. J. Weida, and S. Ogawa, J. Phys. Chem. B **105**, 6767 (2001).
[30] M. Bauer, S. Pawlik, and M. Aeschlimann, Phys. Rev. B **60**, 5016 (1999).
[31] J. Zhao, N. Pontius, A. Winkelmann, V. Sametoglu, A. Kubo, A. G. Borisov, D. Sánchez-Portal, V. M. Silkin, E. V. Chulkov, P. M. Echenique, and H. Petek, Phys. Rev. B **78**, 085419 (2008).
[32] Q. B. Lu, D. J. O'Connor, B. V. King, and R. J. MacDonald, Surf. Sci. **347**, L61 (1996).
[33] H. Petek, A. P. Heberle, W. Nessler, H. Nagano, S. Kubota, S.

Matsunami, N. Moriya, and S. Ogawa, Phys. Rev. Lett. **79**, 4649 (1997).
[34] J. P. Gauyacq and A. K. Kazansky, Phys. Rev. B **72**, 045418 (2005).
[35] J. P. Gauyacq and A. K. Kazansky, Surf. Sci. **601**, 5473 (2007).
[36] See e.g. P. Lazić, V. M. Silkin, E. V. Chulkov, P. M. Echenique, and B. Gumhalter, Phys. Rev. Lett. **97**, 086801 (2006).
[37] See, e.g., C. Cohen-Tannoudji, J. Dupont-Roc, and G. Grynberg, *Processus d'interaction Entre Photons et Atomes* (EDP Sciences/CNRS Editions, Les Ulis, 2001).
[38] M. Bauer, M. Wessendorf, D. Hoffmann, C. Wiemann, A. Mönnich, and M. Aeschlimann, Appl. Phys. A: Mater. Sci. Process. **80**, 987 (2005).
[39] R. Paniago, R. Matzdorf, G. Meister, and A. Goldmann, Surf. Sci. **336**, 113 (1995).
[40] G. K. Wertheim, D. M. Riffe, and P. H. Citrin, Phys. Rev. B **49**, 4834 (1994).
[41] A. K. Kazansky, A. G. Borisov, and J. P. Gauyacq, Surf. Sci. **577**, 47 (2005).
[42] N. Fischer, S. Schuppler, T. Fauster, and W. Steinmann, Surf. Sci. **314**, 89 (1994).
[43] H. Petek, M. J. Weida, H. Nagano, and S. Ogawa, Science **288**, 1402 (2000).
[44] A. G. Borisov, A. K. Kazansky, and J. P. Gauyacq, Phys. Rev. B **64**, 201105 (2001).
[45] U. Bovensiepen, S. Declair, M. Lisowski, P. A. Loukakos, A. Hotzel, M. Richter, A. Knorr, and M. Wolf, Phys. Rev. B **79**, 045415 (2009).